Int. J. Nano Dimens., 11 (1): 58-73, Winter 2020

ORIGINAL ARTICLE

Synthesis and characterization $ZnFe_2O_4$@MnO and $MnFe_2O_4$@ZnO magnetic nanocomposites: Investigation of photocatalytic activity for the degradation of Congo Red under visible light irradiation

Azam Zamani [1], Mirabdullah Seyed Sadjadi [1,], Alireza Mahjoub [2,*], Mohammad Yousefi [3], Nazanin Farhadyar [4]*

[1]*Department of Chemistry, Science and Research Branch, Islamic Azad University, Tehran, Iran*

[2]*Department of Chemistry, Tarbiat Modares University, Tehran, Iran*

[3]*Department of Chemistry, Yadegar-e-Imam Khomeini (RAH) Shahre Rey Branch, Islamic Azad University, Tehran, Iran*

[4]*Department of Chemistry, Varamin Pishva Branch, Islamic Azad University, Varamin, Iran*

Received 05 September 2019; revised 04 November 2019; accepted 11 November 2019; available online 12 November 2019

Abstract

In the present investigation, $ZnFe_2O_4$@MnO and $MnFe_2O_4$@ZnO magnetic nanocomposites were fabricated by facile hydrothermal method and were calcined at 300 °C for 3 h. Synthesis of $ZnFe_2O_4$@MnO and $MnFe_2O_4$@ZnO magnetic nanocomposites optimized by the different weight percentages. The synthesized photocatalyst was characterized by X-ray diffraction (XRD), Fourier transform infrared (FT-IR), Vibrating Sample Magnetometer (VSM), EDAX (Energy dispersive X-ray Analysis), diffuse reflectance UV-vis spectroscopy (DRS) and field emission scanning electron microscopy (FESEM). The $ZnFe_2O_4$@MnO nanoparticles were found to have a size of 20-50 nm. Magnetic studies revealed that the $ZnFe_2O_4$@MnO and $MnFe_2O_4$@ZnO nanocomposites can be easily separated from the solution by an external magnetic field. The photocatalytic degradation of Congo red dye (CR) was investigated based on the removal of Congo red (CR) in aqueous solution in 35 min of visible light irradiation. Compared with $MnFe_2O_4$@ZnO nanocomposite, the $ZnFe_2O_4$@MnO nanocomposite displayed highly photocatalytic performance on the photodegradation of Congo red. Effect of reaction time, pH, and loading of ZnO on degradation of CR was studied,The results demonstrated that the degradation efficiency of $ZnFe_2O_4$@MnO nanocomposite (98.5%) was better than that of $MnFe_2O_4$@ZnO nanocomposite (90.32%), which is due to the presence of narrow band gap energy of $ZnFe_2O_4$@MnO.Kinetics studies have displayed that the degradation of CR by the prepared of photocatalysts follows the pseudo-first-order kinetics and the rate constant achieved for $ZnFe_2O_4$@MnO ($k=0.0371\ min^{-1}$) was much greater than of $MnFe_2O_4$@ZnO ($k=0.0321\ min^{-1}$). The synthesized $ZnFe_2O_4$@MnO nanocomposite can be potentially applied as a magnetically separable photocatalyst to deal with water pollution problems.

Keywords: *Congo Red; Hydrothermal Method; Magnetical Nanocomposites; Photocatalytic Activity; Visible Light.*

How to cite this article

Zamani A, Seyed Sadjadi M, Mahjoub A, Yousefi M, Farhadyar N. Synthesis and characterization $ZnFe_2O_4$@MnO and $MnFe_2O_4$@ZnO magnetic nanocomposites: Investigation of photocatalytic activity for the degradation of Congo Red under visible light irradiation. Int. J. Nano Dimens., 2020; 11 (1): 58-73.

INTRODUCTION

Dyes are one of the largest groups of organic compounds that exhibit an increasing environmental risk. Textile industries are the most common sectors in the world which uses dye to color the fabrics [1-3]. Waste waters generated by the textile industries contain significant amounts of non-fixed dyes, especially of azo dyes, and huge amount of inorganic salts. In addition to the drinkable water shortage and drought in the various region of the global, such as water contamination threats to human health [4]. Hence the removal of these dyes from waste water is a main environmental trouble because conventional

* Corresponding Author Email: *m.s.sadjad@gmail.com*

physicochemical and biological treatment methods are ineffective for decolorization and degradation. Many chemical and physical techniques containing adsorption, coagulation, precipitation, filtration, electrodialysis, membrane separation and oxidation have been utilized efficiently for removal of dye pollutants [5]. Nonetheless, they are non destructive, since they transfer organic compounds from water to another phase, thus causing secondary pollution [6]. Currently, Advanced oxidation processes (AOP's) in which heterogeneous photocatalysis emerges as an appearing harmful method, leading to mineralization of organic water pollutants is widely used [7]. To find an efficient and economically permanent solution to eliminating the water contaminants becomes a pressing subject for every nation. Many research converts to the solar energy, the radiant light, and heat from the sun, which is the most plenty clean energy sources on the Earth. Extensive research studies concentrate on the progress of new materials that can efficiently product solar irradiation and apply it for green environmental contamination management. The photocatalysis process that uses such renewable solar energy to activate the chemical reactions by oxidation and reduction process becomes a sustainable and attractive technology to develop a viable solution for environmental problems [8]. Magnetic and non-magnetic nanoparticles as photocatalysts were made to use in photocatalysis studies. A nanocomposite can be useful in separating nanoparticles from the suspension by making them with magnetic nanoparticles [9-10]. Recently, Magnetic nanoparticles (MNPs) have been attracting a tremendous consideration for their potential use in biomedical applications like controlled drug delivery, cell separation, magnetic resonance imaging and localized hyperthermia therapy of cancer. Iron oxide based magnetic nanoparticles are of special importance because of their suitable biocompatibility and low toxicity. Iron oxides are very ordinary compounds and they are widespread in nature and readily synthesized in the laboratory. In almost everywhere of the global system atmosphere, biosphere, hydrosphere, and lithosphere, iron oxides present. The future of the data storage industry will be worth of wondering by looking at the options available today and the development during the time. Manganese ferrite ($MnFe_2O_{4)}$ is extraordinarily significant member of the ferrite family with a variety of utilizations in the modern era of science and engineering [11]. Zinc Ferrite ($ZnFe_2O_4$) displays superparamagnetic behavior and it has potential application in many fields, such as photocatalysis, magnetic resonance imaging (MRI), Li-ion batteries and gas sensors [12]. Various semiconductor photocatalysts have been considered for the degradation of organic pollutants. Among them, manganese oxide (MnO) is a semiconductor with a wide band gap width (3.9 ±4/0eV) at room temperature [13]. Manganese oxides, including MnO, MnO_2, and Mn_3O_4, are interesting composites and have been applied in wastewater treatment, catalysis, sensors, supercapacitors, and alkaline and rechargeable batteries [14]. Also, Zinc oxide (ZnO) is a semiconductor with a wide band gap width (3.37 eV) and large excitation binding energy (60 meV) at room temperature, which lead to ZnO has been employed considerable in the degradation of dye pollutant [15]. Despite a large number of studies published on nanocomposites photocatalytic activity, fabrication of $ZnFe_2O_4$@MnO and $MnFe_2O_4$@ZnO magnetic nanocomposites via facile hydrothermal method has not yet been reported. And also, we investigated the photocatalytic activity of magnetic nanocomposites for degradation of Congo red dye under the visible light irradiation In the present study, the magnetic nanocomposites display a high photocatalytic activity under the influence of visible light irradiation at a shorter irradiation time. Furthermore, we have fabricated $ZnFe_2O_4$@MnO and $MnFe_2O_4$@ZnO nanocomposites by hydrothermal method and samples were calcined at 300 °C for 3 h with smaller particle size. Our synthesis of $ZnFe_2O_4$@MnO and $MnFe_2O_4$@ZnO nanocomposites modified by the different weight percentages of the prepared samples. And also, Effect of reaction time and pH on degradation of CR was investigated. Synthesized nanocomposites were characterized by using XRD, FT-IR, EDAX, UV-DRS, FESEM and VSM. The photocatalytic activity was investigated in an aqueous solution for the photocatalytic degradation of Congo red with the visible light irradiation.

EXPERIMENTAL

Materials

All the chemicals that were employed in the experiments were reagent grade such as 20% NaOH (Merck, Germany), $Mn(NO_3)_2$ (Merck, Germany), $Zn(NO_3)_2$ (Merck, Germany) and

$Fe(NO_3)_3$ (Merck, Germany). All the experiments were performed in aqueous media.

Instrumentation

The crystalline structure of $MnFe_2O_4$@ZnO and $ZnFe_2O_4$@MnO were investigated by XRD (Philips PW 1730 Japan model) with CuK_α radiation (1.5406) ˚A in2θ scan range of 10–80°. In order to examine the morphologies of $MnFe_2O_4$@ ZnO and $MnFe_2O_4$@ZnO nanomaterials, FESEM measurements were done with a ZEISS DSM-960A analytic microscope (Germany). The magnetic hysteresis loops of samples were performed by a vibrating sample magnetometer with VSM, Lake Shore Model 7404 at room temperature (300 K). Then, A diffuse reflectance spectrum (DRS) of the $MnFe_2O_4$@ZnO/GO and $MnFe_2O_4$@ZnO/RGO nanocomposites were recorded on a UV-2550 Shimadzu UV–vis spectrophotometer equipped with ISR-2200 DRS accessory (UV-2550 Shimadzu, Japan). Finally, IR spectra were recorded on a Bruker FT-IR instrument using KBr plates.

Synthesis of the $MnFe_2O_4$@ZnO nanoparticles

The fabrication of $MnFe_2O_4$@ZnO was carried out by hydrothermal method [16]. In this regard, 4.75 g Mn $(NO_3)_2$,5.87 g Fe $(NO_3)_3$ and 10% NaOH dissolved in 40 ml of distilled water were mixed under magnetic stirring for 30 min. Then, transferred to 50 ml of Teflon lined autoclave and heated to 150 °C for 3 h under autogenous pressure. The reaction mixture was allowed to cool to room temperature. Finally the precipitated solution was washed several times with distilled water and ethanol. Then the brown precipitates were collected and dried at 70°C for 3 hours in hot air oven. Moreover, 1 g of ZnO was calcined at 500 °C for 3 h, followed by dropwise addition of 10%

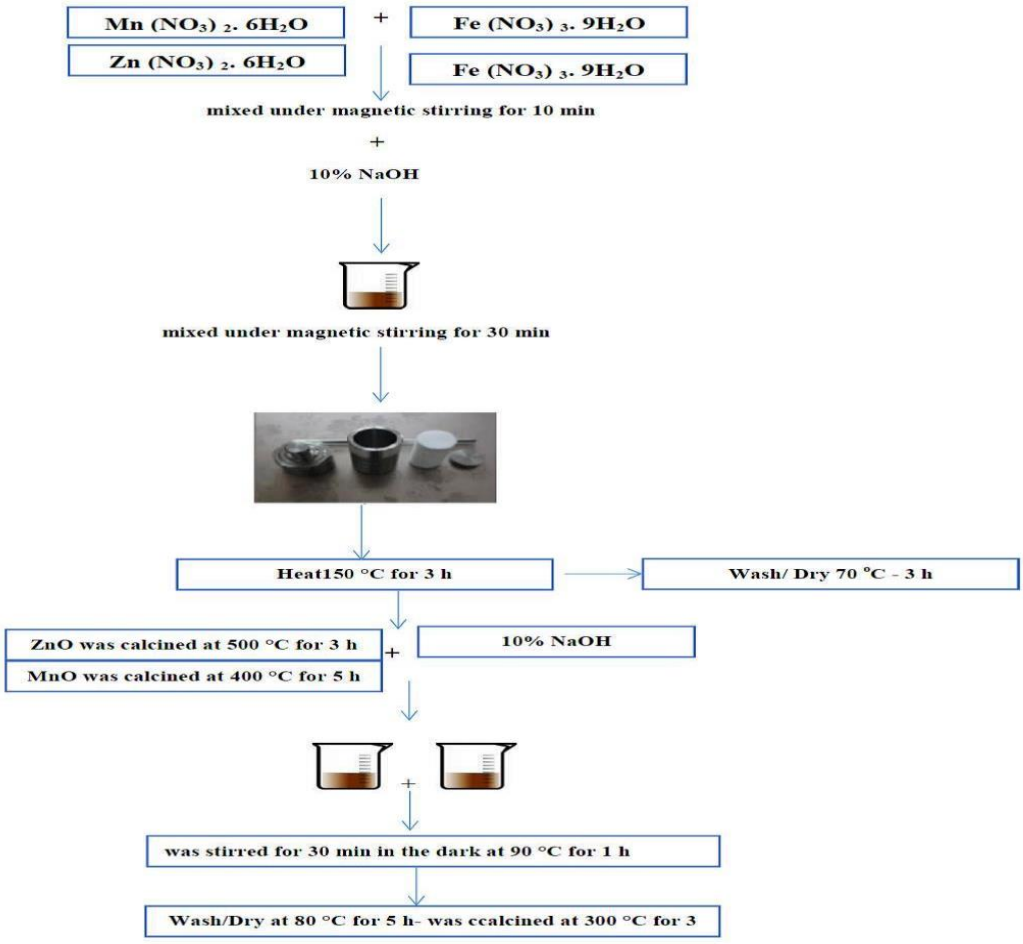

Fig. 1. The preparation steps of $MnFe_2O_4$@ZnO and $ZnFe_2O_4$@MnO nanocomposites.

NaOH solution in calcined ZnO and magnetically stirred for 10 min. After the Mn?Fe precursor solution was added to the suspension, the new mixture was stirred for 30 min in the dark at 90 °C for 2 h. In the following stage, the obtained precipitate was filtered and washed with ultrapure water for various times and was allowed to dry in a vacuum oven at 80 °C for 5h. Finally, the product was calcined at 300 °C for 3 h to form $MnFe_2O_4$@ ZnO nanoparticles.

Synthesis of the $ZnFe_2O_4$@MnO nanoparticles

$ZnFe_2O_4$@MnO nanoparticles are synthesized by a hydrothermal method [16]. In this consideration, 3.75 g Zn $(NO_3)_2$,4.87 g Fe $(NO_3)_3$ d and 10% NaOH dissolved in 50 ml of distilled water were mixed under magnetic stirring for 30 min. Then, Then, transferred to 50 ml of Tteflon lined autoclave and heated to 150 °C for 3 h under autogenous pressure. The reaction mixture was allowed to cool to room temperature. Finally the precipitated solution was washed several times with distilled water and ethanol. Then the solution was collected and dried at 70°C for 3 hours in hot air oven. Furthermore,1 g of MnO was calcined at 400 °C for 5 h. Then, the calcined MnO was added to 10% NaOH solution and magnetically stirred for 10 min. After the Zn–Fe precursor solution was added to the suspension, the new solution was stirred for 30 min in the dark at 90 °C for 2 h. The resulting precipitate was filtered, followed by washing with ultrapure water for several times and was allowed to dry in a vacuum oven at 80 °C for 5h. Finally, the obtained product calcined at 300 °C for 3 h to form $ZnFe_2O_4$@MnO nanoparticles. Fig. 1, displays the preparation steps of $MnFe_2O_4$@ZnO and $ZnFe_2O_4$@MnO nanocomposites.

Photocatalytic degradation experiments

The Photocatalytic activity of the as-prepared samples were measured by monitoring the degradation rate of CR solution as a model organic pollutants**.** The experiment was performed under visible light using a 100 W tungsten lamp as a visible light source. The photocatalytic experiments were performed at 25 °C with a concentration of 0.10 g L^{-1} $MnFe_2O_4$@ZnO and $ZnFe_2O_4$@MnO nanocomposites and 50 mg L^{-1} of CR solution with time intervals of (5–35 min) at pH= 4. In this experiment, 0.10 g L^{-1} of $MnFe_2O_4$@ ZnO and $ZnFe_2O_4$@MnO nanocomposites was added to 100 ml of 50mg L^{-1} CR solution. Before the photocatalytic reaction, the suspension was stirred in the dark for 30 min for adsorption–desorption equilibrium between the photocatalyst and dye solution. finally, it was irradiated. During irradiation, 5 ml of the suspension was sampled at an interval of 5 min and centrifuged to eliminate the catalyst particles and it was measured by Shimadzu UV-1650PC Model UV-vis spectrophotometer at λ_{max}= 500 nm. The dye degradation percentage was obtained from the following equation (1):

$$\text{The degradation efficiency (\%) of CR} = (C_0\text{-}C) / C_0*100 \quad (1)$$

where C_0 represents the initial CR concentration (mg/L) and C indicates the CR concentration at a certain reaction time (min).

RESULTS AND DISCUSSION

Structural study

XRD patterns of synthesized $MnFe_2O_4$@ ZnO and $ZnFe_2O_4$@MnO was studied by X-ray diffraction Philips Xpert XRD. **Fig. 2** displays the X-ray diffraction patterns in the 2θ ranges from 5 to80° for $MnFe_2O_4$@ZnO and $ZnFe_2O_4$@MnO. The average crystallite size for prepared samples from the range of 20 nm to 50 nm was computed by using standard Debye-Scherrer equation D=0.9λ/(βcosθ) [17], where D demonstrates the diameter of the nanoparticles, λ (Cu Kα) =1.5406 A° and β represents the full-width at half maximum of the diffraction lines. **Fig.2a** and **Fig.2b** illustrates the X-ray diffraction pattern of the $ZnFe_2O_4$@MnO and $MnFe_2O_4$@ZnO, respectively. As portrayed in **Fig.2a**, diffraction peak of $ZnFe_2O_4$@MnO was observed at the angles of 18.24, 57.42 and 75.50° , which corresponds to the (111), (511) and (171), respectively. Based on the results, The peaks centered at the angles of 35.34, 56.79, 62.36 and 73.76° indicated (311), (511), (400) and (533) corresponded to the cubic phase of $ZnFe_2O_4$. These diffraction peaks were remarkably resembled with the standard JCPDS No. 98-003-0547. The peaks centered at the angles of 29.96,33.52,37.88, 42.19, 57.84, 64.43and 65.38° indicated (023), (113), (006), (220), and (212) concurred to the cubic phase of MnO which were directly indexed to JCPDS No. 01-075-0257. The X-ray diffraction pattern of $MnFe_2O_4$@ZnO was observed in Fig.2b. The peaks centered at the angles of 35. 39, 42.93 and 62.30° indicated(113), (004) and (022) respectively, which corresponded to $MnFe_2O_4$@ZnO. Based on

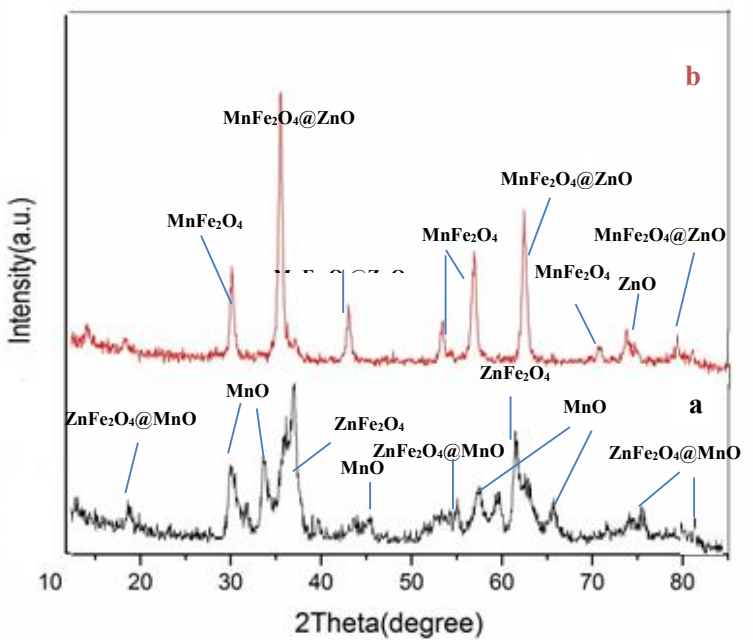

Fig. 2. XRD patterns for (a) $ZnFe_2O_4$@MnO and (b) $MnFe_2O_4$@ZnO.

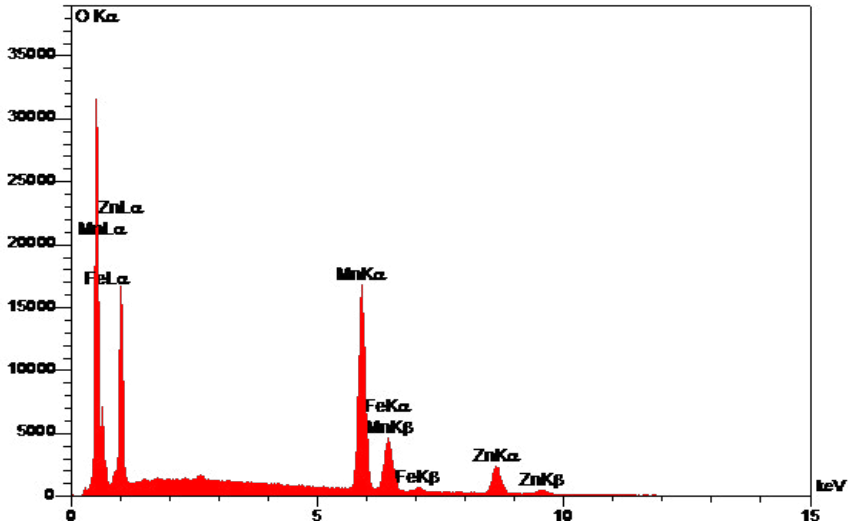

Fig. 3. EDAX analyses of $ZnFe_2O_4$@MnO nanocomposite.

the results, The peaks centered at the angles of 18.23, 29.99, 35.33,53.26, 56.77, 70.71 and 74.73 ° indicated (111), (022), (113), (224), (115), (026) and (226) where the $MnFe_2O_4$ belongs to the cubic phase and diffraction peaks were directly indexed to JCPDS No. 98-006-2998. The peaks centered at the angles of 36.94,42.92,62.31, 74.70and 78.64° indicated (111), (002), (022), (113) and (222) corresponded to the cubic phase of ZnO which were directly indexed to JCPDS No. 98-011-6320. As depicted in **Fig. 2b,** the The closer study of EDAX data reveals that Zn, Fe, Mn and O elements were clearly present in the $MnFe_2O_4$@ZnO and $ZnFe_2O_4$@MnO nanocomposites, respectively. The amounts of elements are reported for the nanocatalyst $MnFe_2O_4$@ZnO and $ZnFe_2O_4$@MnO

Table 1. EDX quantification elements of $ZnFe_2O_4$@MnO nanocomposite.

Element	O	Mn	Fe	Zn	Total
W%W%	40.71	42.12	7.81	9.36	100.00
Atom%	70.80	21.33	3.89	3.98	100.00

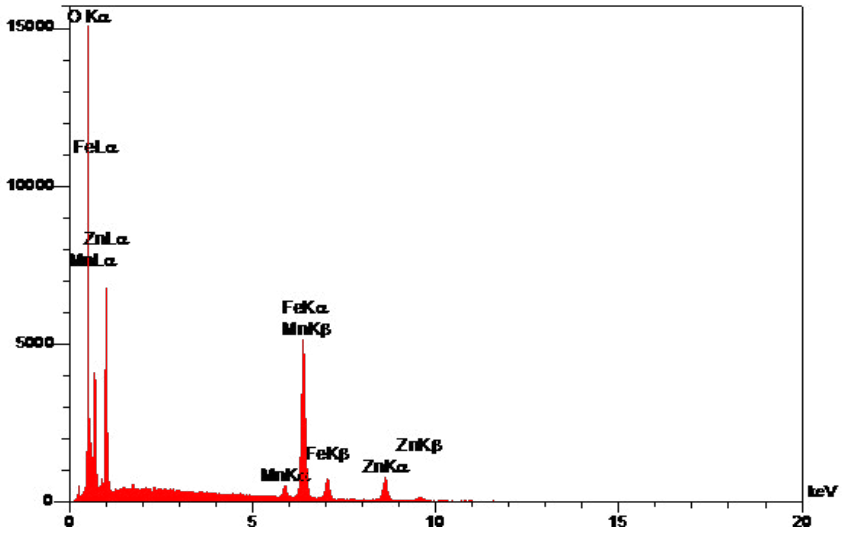

Fig. 4. EDAX analyses of $MnFe_2O_4$@ZnO nanocomposite.

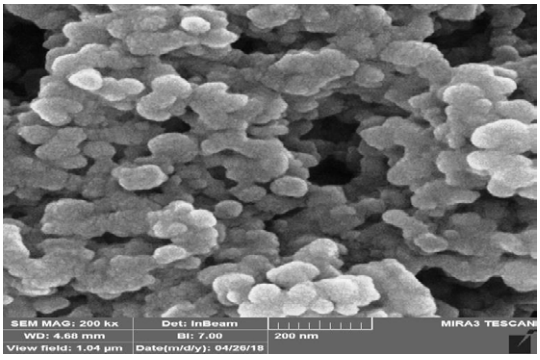

Fig. 5. FESEM image of $ZnFe_2O_4$@MnO nanoparticles.

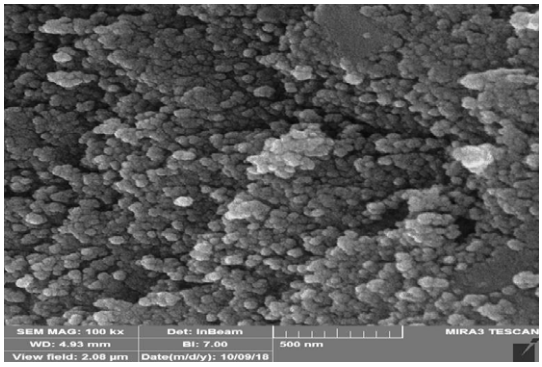

Fig. 6. FESEM image of $MnFe_2O_4$@ZnO nanoparticles.

in Tables 1 and2, respectively. Furthermore, as shown in **Fig.3** and **Fig.4**, the surface morphology and its chemical composition of the synthesized photocatalyst were examined by using FESEM image. Based on the results, **Figs. 5** and **6** reveal the agglomerated spherical shape of $ZnFe_2O_4$@ MnO and $MnFe_2O_4$@ZnO nanocomposites with an average particle size of < 100 nm, respectively.

Infrared spectral study

FT-IR analysis was done for a detailed investigation of the obtained samples in the synthesized $MnFe_2O_4$@ZnO and $ZnFe_2O_4$@MnO as portrayed in Fig. 7. As shown in Fig. 8a, the solid state FT-IR spectra of the nanocomposites indicated a low intensity bands in the range of 480 and 507 cm^{-1} were assigned to Zn–O and Mn–O stretching vibration band in $ZnFe_2O_4$@MnO respectively. In addition, another peak appeared at the 650–540 cm^{-1}, which could assigned to the Fe–O stretching. The absorption band around 1707cm^{-1} assigned to stretching vibration of carbonyl group C-O. The stretching vibration of the carboxylate group C=O is observed around 1459 cm^{-1}. Also, The bending vibration of H-O-H group appeared at 1625cm^{-1}. The band at 3500-3200 cm^{-1} is attributed to the stretching and bending modes of free and absorbed water

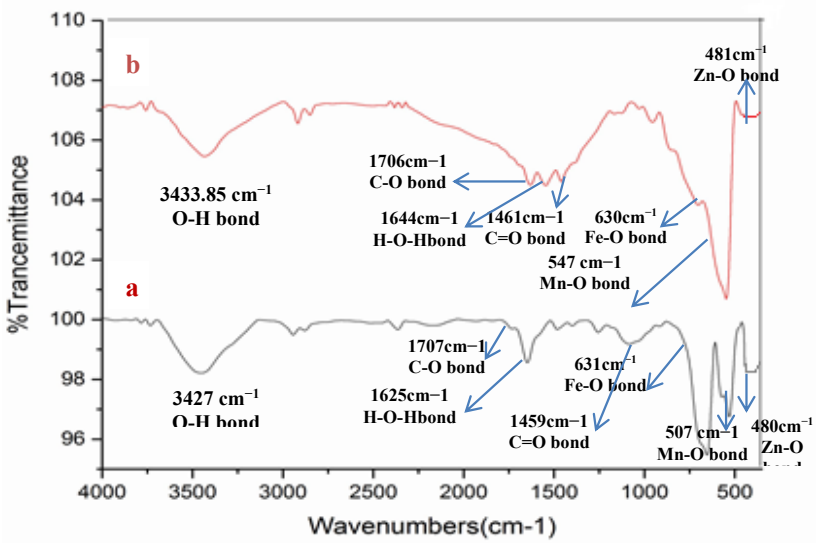

Fig. 7. FT-IR spectra of prepared (a) $ZnFe_2O_4$@MnO and (b) $MnFe_2O_4$@ZnO nanoparticles.

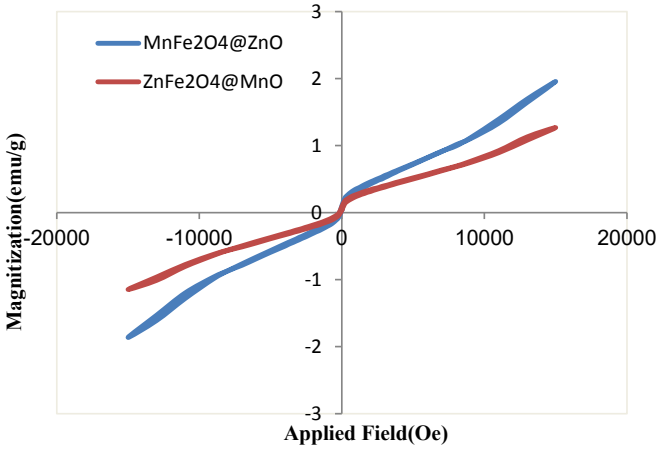

Fig. 8. Hysteresis curves of $MnFe_2O_4$@ZnO and $ZnFe_2O_4$@MnO nanocomposites.

on the surface of the prepared $ZnFe_2O_4$@MnO nanoparticles [18]. As shown in Fig. 8b, the solid state FT-IR spectra of the nanoparticles displayed a low intensity bands in the range of 481 and 547 cm^{-1} were attributed to Zn–O and Mn–O stretching vibration band in $MnFe_2O_4$@ZnO. Furthermore, another peak observed at the 650–500 cm^{-1} which could be assigned to the octahedral group Fe-O. The absorption band around 1706cm^{-1} assigned to stretching vibration of carbonyl group C-O. The stretching vibration of the carboxylate group C=O is shown around 1461 cm^{-1}. Also, The bending vibration of H-O-H group appeared at 1644cm^{-1}. The broad peak at 3433.85cm^{-1} is assigned to the stretching and bending modes of free and absorbed water on the surface of the synthesized $MnFe_2O_4$@ZnO nanocomposites [19-20]. The FT-IR spectra confirm the presence of organic impurities in the synthesized samples due to the preparation conditions.

Magnetic properties of $MnFe_2O_4$@ZnO and $ZnFe_2O_4$@MnO

The magnetization measurement for the as-prepared $MnFe_2O_4$@ZnO and $ZnFe_2O_4$@MnO nanoparticles was carried out using a vibrating sample magnetometer (VSM) at room temperature. The magnetic hysteresis loops of the synthesized $MnFe_2O_4$@ZnO and $ZnFe_2O_4$@MnO nanocomposites is observed in Fig. 8, which confirms that the resulting samples showed a characteristic of the superparamagnetic behavior

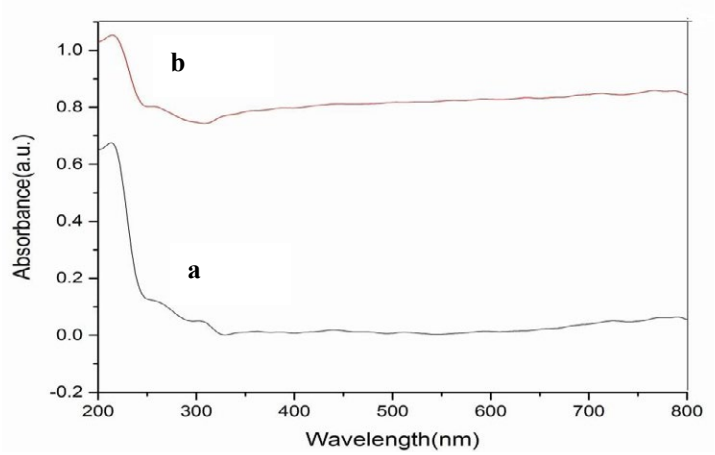

Fig. 9. Optical Absorption Spectrum Of (a) $ZnFe_2O_4$@MnO and (b) $MnFe_2O_4$@ZnO.

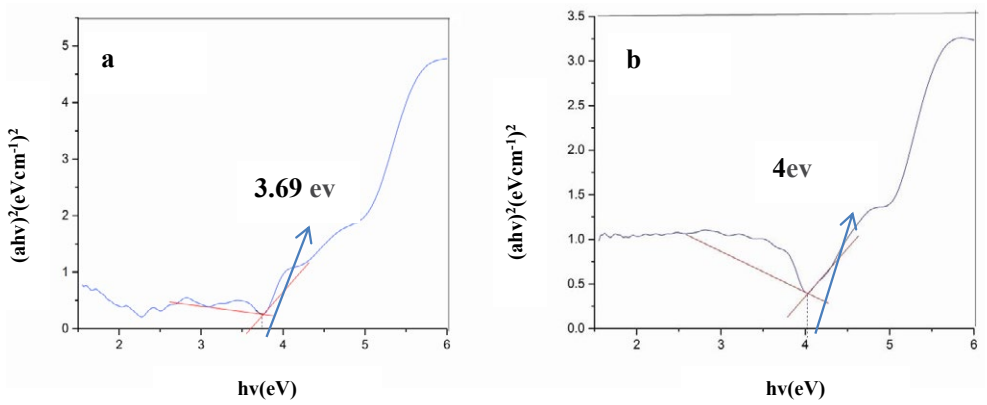

Fig. 10. DRS plots of $(ahv)^2$vs. photon energy hv(eV) for (a) $ZnFe_2O_4$@MnO and (b) $MnFe_2O_4$@ZnO.

with the saturation magnetization of 1.95 and 1.26 emu g^{-1} of $MnFe_2O_4$@ZnO and $ZnFe_2O_4$@MnO nanocomposites, respectively. also, the remanent magnetization of $MnFe_2O_4$@ZnO and $ZnFe_2O_4$@MnO is 0.102 and 0.089 emu g^{-1}, respectively. Finally, The results demonstrated the superparamagnetic behavior of the nanocomposites because of a decrease in the particle size below a critical value (lower than 100 nm). Thus, the size of the crystalline nature influences the magnetic properties of the nanoparticles [21].

Optical analysis of $ZnFe_2O_4$@MnO and $MnFe_2O_4$@ZnO

The optical absorption property relevant to the electronic structure formation is indicated as a key factor in demonstrating the photocatalytic activity [22]. The optical properties of the prepared $MnFe_2O_4$@ZnO and $ZnFe_2O_4$@MnO samples were performed by the diffused reflectance UV-vis spectra (DRS), as shown in Fig. 9. The UV-Visible absorption spectra of the synthesized nanocomposites recorded in the range of wavelength 200-800 nm. According to the spectra, all synthesized samples indicated photoabsorption from UV light to visible light region, which displays the possibility of high photocatalytic activity of these nanocomposites under visible light. The band gap of the synthesized nanomaterials calculated from the plot of the transformed Kubelka-Munck function vs. the energy of light [23] is observed in Fig.10. The optical band gap energies of the synthesized $MnFe_2O_4$@ZnO and $ZnFe_2O_4$@MnO nanocomposites are 4and 3.69 eV, respectively. But, this band gap is yet so large that visible light irradiation ($\lambda > 420$ nm) cannot photoexcite electrons in the valence band (VB)

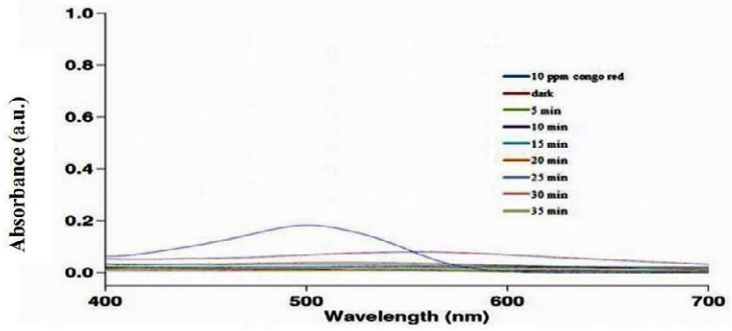

Fig. 11. Photocatalytic degradation of Congo red under visible light in presence of $ZnFe_2O_4$@MnO.

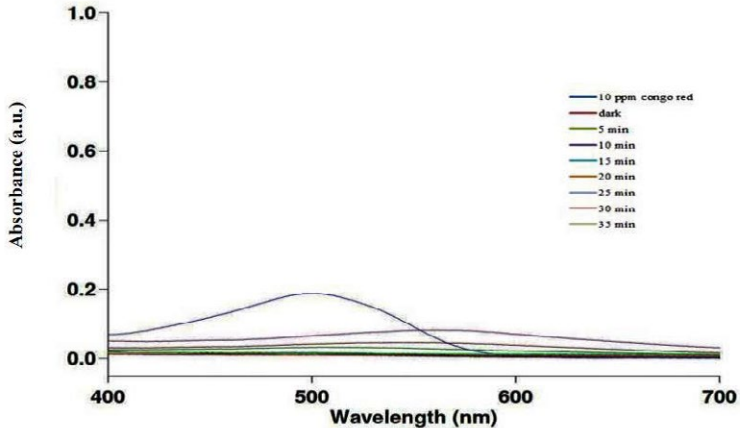

Fig. 12. Photocatalytic degradation of Congo red under visible light in presence of $MnFe_2O_4$@ZnO.

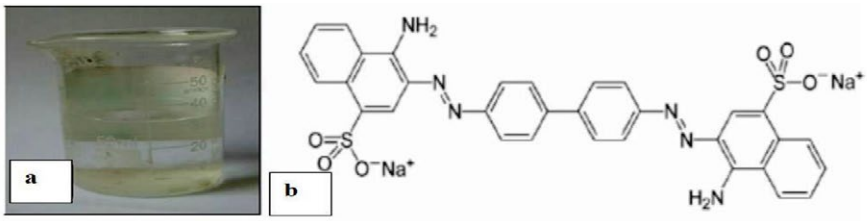

Fig. 13. (a) The degradation of congo red dye [pH region (13-14)] and (b) congo red structure with two sulfonic groups.

to the conduction band (CB) of $ZnFe_2O_4$@MnO. Based on the experimental results, an electron transport mechanism for the photodegradation of the $ZnFe_2O_4$@MnO composites is suggested. The MnO nanoparticle with a wide band gap of ~3.90 eV, is difficult to reach excited states under visible light irradiation. In this work, $ZnFe_2O_4$ act as an electron transfer channel in the $ZnFe_2O_4$@MnO composite. Therefore, The results revealed that the addition of $ZnFe_2O_4$ can narrow the band gap of MnO (3.9 ± 0/4eV) to the visible light region of ~3.69ev, which improved the electron–hole separation, leading to enhanced photocatalytic efficiency [13]. Additionally, the addition of $MnFe_2O_4$ to ZnO structure (3.37ev) causes an increase the band gap width of $MnFe_2O_4$@ZnO to 4eV for $MnFe_2O_4$@ZnO. Thus, this band gap is so large that visible light irradiation (λ > 420 nm) cannot photoexcite electrons in the valence band (VB) to the conduction band (CB) of $MnFe_2O_4$@ZnO [15].

Photocatalytic degradation activities of $MnFe_2O_4$@ZnO and $ZnFe_2O_4$@MnO nanocomposites

The photocatalytic activity of synthesized $MnFe_2O_4$@ZnO and $ZnFe_2O_4$@MnO nanocomposites was investigated by using CR dye solutions as a model organic pollutant under visible illumination,

Table 2. EDX quantification elements of $MnFe_2O_4$@ZnO nanocomposite.

Element	O	Mn	Fe	Zn	Total
W%W%	48.09	2.32	42.33	7.26	100.00
Atom%	76.74	1.08	19.35	2.83	100.00

Table 3. Compare the degradation rate, (D%) of $ZnFe_2O_4$@MnO nanocomposite (0.05-0.20g).

Catalysts	D% 5 min	D% 10 min	D% 15 min	D% 20 min	D% 25 min	D% 30min	D% 35 min
$ZnFe_2O_4$@MnO(0.05g)	23.88	33.54	43.23	50.42	54.88	60.31	62.33
$ZnFe_2O_4$@MnO(0.1g)	20.23	30.42	40.15	59.25	70.38	85.25	98.5
$ZnFe_2O_4$@MnO(0.15g)	10.12	20.23	30.15	40.50	52.19	61.46	85.33
$ZnFe_2O_4$@MnO(0.20g)	22.30	35.18	42.55	54.42	59.88	63.33	69.75

Table 4. Compare the degradation rate, (D%) of $MnFe_2O_4$@ZnO nanocomposite (0.05-0.20g).

Catalysts	D% 5 min	D% 10 min	D% 15 min	D% 20 min	D% 25 min	D% 30min	D% 35 min
$MnFe_2O_4$@MnO(0.05g)	15.88	38.15	48.24	53.37	50.88	58.33	65.42
$MnFe_2O_4$@ZnO(0.1g)	10.15	20.28	45.56	58.25	78.15	82.23	90.32
$MnFe_2O_4$@ZnO(0.15g)	15.32	25.14	38.15	44.28	55.33	68.23	75.55
$MnFe_2O_4$@ZnO(0.20g)	22.31	28.19	32.12	38.15	45.55	58.23	68.32

as shown in Figs. 11 and 12. In this regard, 100 ml of 50 mg/l CR solution under pH=13-14 with the presence of 0.10g $MnFe_2O_4$@ZnO and $ZnFe_2O_4$@MnO nanocomposites were exposed to the visible light for 35 min. The experiments demonstrated that the percentage of maximum dye degradation in the presence of 0.10g $MnFe_2O_4$@ZnO and $ZnFe_2O_4$@MnO nanocomposites were 90.32 % and 98.50 % respectively. The Congo red (CR) main absorption peak happens at 498 nm. The degradation rate was calculated by decreasing in peak intensity at 498 nm in Figs. 11 and 12. When $MnFe_2O_4$@ZnO and $ZnFe_2O_4$@MnO nanocomposites are added into solution and exposed to sunlight for 35 minutes, peak intensity gradually decreases. The degradation rate for $ZnFe_2O_4$@MnO is much higher than $ZnFe_2O_4$@MnO, as shown in Tables 3 and 4. To study the effect of pH, several experiments were performed on photocatalyst. The pH of the CR dye solution 50ppm is about 7 in the presence of nanocomposites. Calculation of the effect of pH was carried out in the range of 1-14 by adding sodium hydroxide and hydrochloric acid. In the case studies, it was observed that in the pH=1-7, all photocatalysts can only absorb the Congo red, but it does not have the degradation ability and the least photocatalytic activity was found in the pH regions 8-12. In alkaline pH region 13-14 the degradation of Congo red dye was observed (Fig. 13a). This phenomenon can be illustrated by the surface properties of the $MnFe_2O_4$@ZnO and $ZnFe_2O_4$@MnO nanocomposites. Two sulfonic acid groups of Congo red can ionize and make a Congo red anion (Fig. 13 -b). The $ZnFe_2O_4$@MnO photocatalyst in the high acidic regions (pH=1-7) has a positive small surface potential (Zeta-point charge = +5.84) and in the highly alkaline regions (pH=13-14) has a very high positive surface potential (Zeta-point charge = +15.8). And also, $MnFe_2O_4$@ZnO photocatalyst in the high acidic regions (pH=1-7) has a positive small surface potential (Zeta-point charge = +3.84) and in the highly alkaline regions (pH=13-14) has a very high positive surface potential (Zeta-point charge = +9.8). A negative surface charge of the Congo red anion is capable to absorb the positive surface of nanocomposite. Therefore, in the region (pH=1-7), photocatalysts only absorbs the Congo red and in the alkaline region (pH=13-14) photocatalysts are capable to degrade the Congo red dye. The photocatalysts in the region between pH=7-13 have a negative surface potential, therefore the interaction and destruction of the Congo red dye in this area has been minimized. The experiments of photocatalysis were carried out at pH= 13-14

owing to this pH is optimized and nanocomposites gave the best efficiency in the photocatalytic degradation of Congo red. $ZnFe_2O_4$@MnO nanocomposite has a very high positive surface potential compared to the $MnFe_2O_4$@ZnO nanocomposite in the highly alkaline regions. Therefore, $ZnFe_2O_4$@MnO photocatalyst gave the best performance in the photocatalytic degradation of Congo red. The effect of initial dye (CR), concentration on its photodegradation was studied from 50-80 ppm at pH=13-14 and nanocomposites dosage of 0.10g/L. It is suggested that the photodegradation decreases with increase of initial CR concentration. At high dye concentrations, the formation reactive oxygen species on the photocatalyst surface is reduced because the photons are interrupted by the dye molecules before they can reach the catalyst surface. Further, nanocomposites dosage is also same for all initial CR concentration and therefore the formation of •OH remains constant [24]. In the case studies, At high dye concentrations owing to it does not have the degradation ability and the least photocatalytic activity was revealed. We don't cite in this research. The tests of photocatalysis were performed in 10mg/l CR solution due to this concentration is optimized and nanocomposites gave the best activity in the photocatalytic degradation of Congo red.

Effect of catlyst dosage

Figs. 14 and 15 show the loading effect of the $MnFe_2O_4$@ZnO and $ZnFe_2O_4$@MnO nanocomposites on the degradation rate of CR solutions. The tests were carried out by varying the weight of photocatalyst from 0.05 g to 0.20 g with optimum CR pH. Based on the results,the

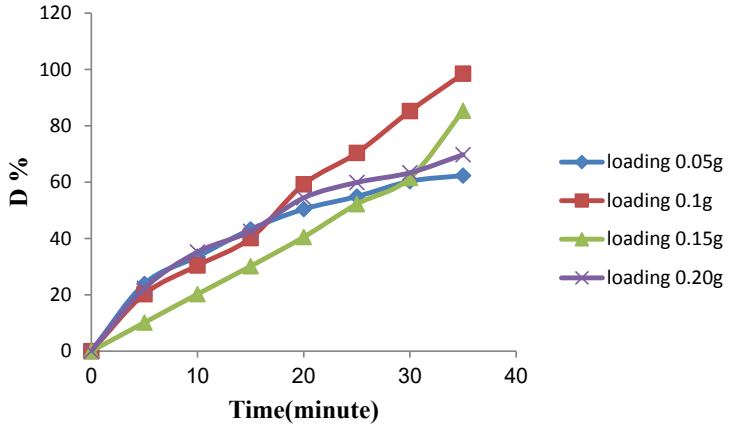

Fig. 14. The effect of loading $ZnFe_2O_4$@MnO nanocomposite on the CR solutions degradation (Sample: 0.050 g $ZnFe_2O_4$@MnO, initial concentration of CR solution: 50 mg/l, pH of CR solution: 13-14, Volume: 100 ml).

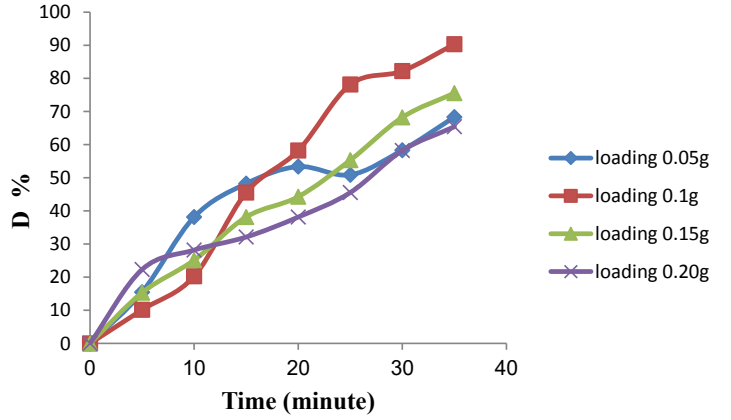

Fig. 15. The effect of loading $MnFe_2O_4$@ZnO nanocomposite on the CR solutions degradation (Sample: 0.050 g $MnFe_2O_4$@ZnO, initial concentration of CR solution: 50 mg/l, pH of CR solution: 13-14, Volume: 100 ml).

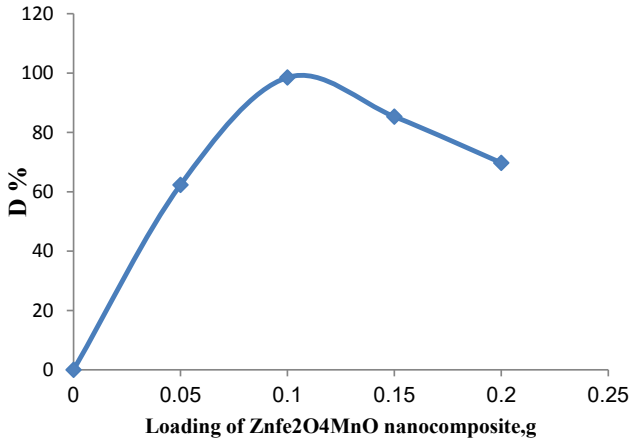

Fig. 16. Relationship between $ZnFe_2O_4$@MnO nanocomposite loading and degradation rate of CR solution.

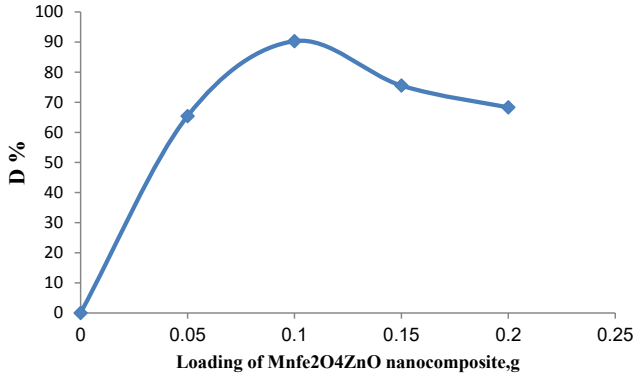

Fig. 17. Relationship between $MnFe_2O_4$@ZnO nanocomposite loading and degradation rate of CR solution.

CR degradation rate of the $ZnFe_2O_4$@MnO and $MnFe_2O_4$@ZnO nanocomposites increased from 62.33% to 98.50% and68.32% to 90.32% , respectively, along with an increase in the weight of the photocatalyst from 0.05 g to0.1 g. However, as shown in Figs.16 and 17, CR degradation rate decreased when the weight increased to 0.15 g and 0.20g. Moreover, agglomeration happened, leading to an increase in the darkness of solution when the loading of nanoparticles surpassed the optimum amount for the reaction. This situation prevented the influence of visible light, which resulted in losing the activated sites of $MnFe_2O_4$@ZnO and $ZnFe_2O_4$@MnO nanocomposites by collision with the ground state $MnFe_2O_4$@ZnO and $ZnFe_2O_4$@MnO nanocatalysts [25]. The photocatalytic degradation of Congo red as a function of time by employing the synthesized $MnFe_2O_4$@ZnO and $ZnFe_2O_4$@MnO nanocomposites was evaluated under visible light irradiation, as shown in Fig. 18. It can be seen that the $ZnFe_2O_4$@MnO nanocomposites compared to $MnFe_2O_4$@ZnO nanocomposites gave the best efficiency in the photocatalytic degradation of Congo red. The enhanced photocatalytic activity of $ZnFe_2O_4$@MnO composite is owing to the well optical absorptions in the UV-Vis region with a lower band gap energy giving rise to a higher photocatalytic efficiency.

Kinetics Studies of $MnFe_2O_4$@ZnO and $ZnFe_2O_4$@MnO nanocomposites

The dyedegradation percentage of the $MnFe_2O_4$@ZnO and $ZnFe_2O_4$@MnO nanocomposites were used from the following equation [25]:

$$R = (C_0 - C_t)\, C_0 \times 100\% \quad (2)$$

Where $C_0$is the initial CR concentration (mg/l) and C_t is the CRconcentration at a certain reaction

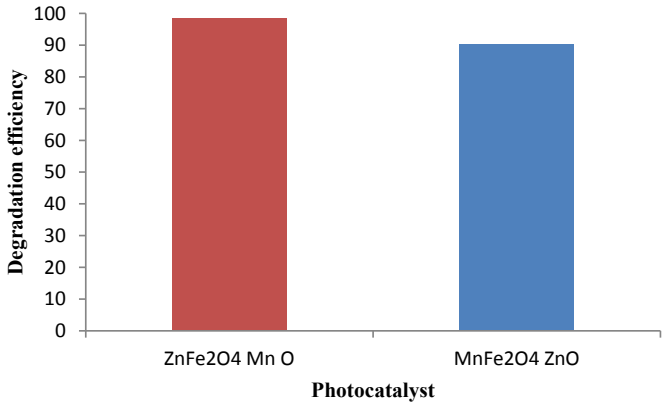

Fig. 18. Comparison of the photodegradation efficiencies of congo red for $ZnFe_2O_4$@MnO and $MnFe_2O_4$@ZnO nanocomposites under visible light irradiation for 35 min.

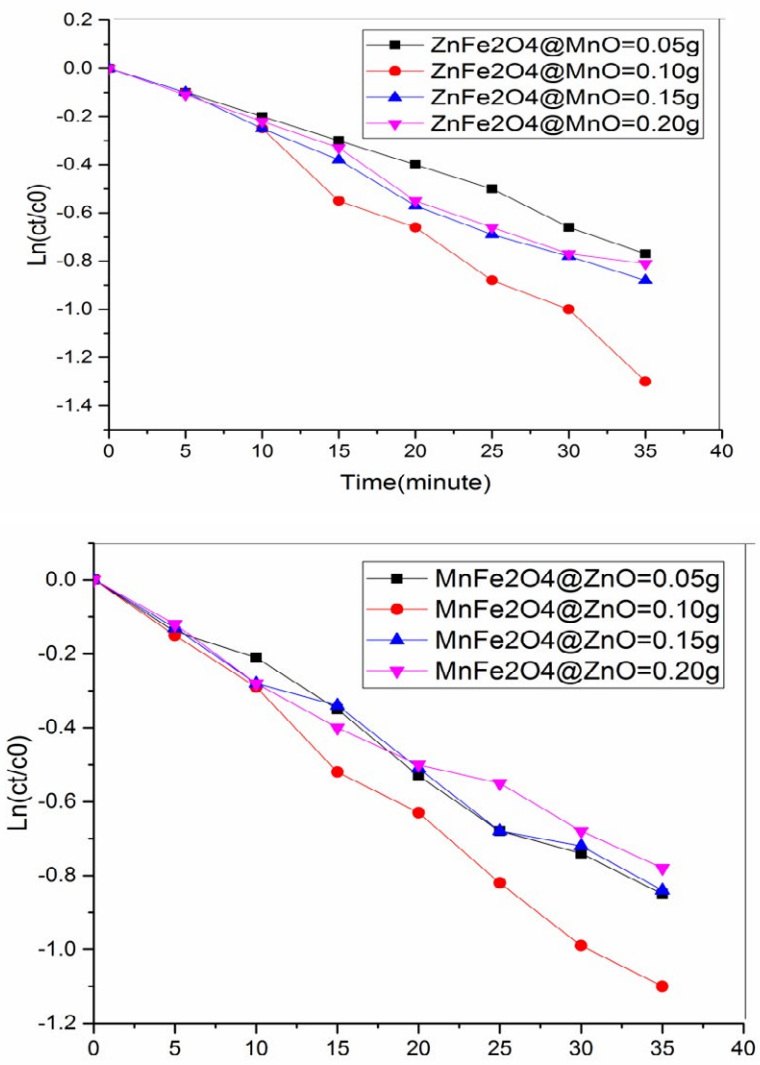

Fig. 19. a) The effect of $ZnFe_2O_4$@MnO catalyst amount on the photocatalytic degradation of Congo red. b) The effect of $MnFe_2O_4$@ZnO catalyst amount on the photocatalytic degradation of Congo red.

time (min). A pseudo first order reaction model with respect to CRconcentration was presumed to evaluate the degradation rate kinetic and rate constant. First order reaction rate equation can be revealed as follows:

$$-d[C]/dt = k[C] \quad (3)$$

Where k = rate constant, min^{-1}This equation can be integrated to acquire an integrated form:

$$\ln C_0/C_t = kt \quad (4)$$

The reaction kinetics of the photocatalysis improved by using the first order kinetic model as follows:

$$\ln C_t = \ln C_o - kt \quad (5)$$

The plot of Ln (C_t/C_o) versus t can be approached as straight lines (Figs. 19a and b), which means that the photodegradation of CR is fitted as pseudo-first-order kinetics. Table 5 and 6 represent the calculated rate constant and the correlation coefficient under different conditions. The effect of the reaction rate of 0.10g $ZnFe_2O_4$@MnO was 0.0371 min^{-1}, which was slightly higher, compared to 0.05g, 0.15g and 0.20g $ZnFe_2O_4$@MnO nanocomposite. Additionally, the effect of the reaction rate of 0.10 g $MnFe_2O_4$@ZnO was 0.0324 min^{-1}, which was some higher, compared to 0.05 g/L and 0.02 g/L the as-synthesized $MnFe_2O_4$@ZnO sample.

Photocatalytic mechanism of $MnFe_2O_4$@ZnO and $ZnFe_2O_4$@MnO nanocomposites

The acceptable photodegradation mechanism by applying as-synthesized $ZnFe_2O_4$@MnO photocatalyst is showed in Fig.20. In this mechanism, the dye molecules adsorbed on the surface of the catalyst absorb visible radiations and undergo electronic excitation from the highest occupied molecular orbital to the lowest unoccupied molecular orbital (LUMO). Then excited electrons from the LUMO of the dye molecule are injected into the conduction band (CB) of the $ZnFe_2O_4$@MnO photocatalyst and the dye is converted into a cationic dye radical. This dye radical undergoes degradation to produce mineralized products. The electron in the CB of the metal oxide is further scavenged by oxygen to produce $\mathbf{O}_2^-$ and results in the decolourisation of dyes. This mechanism is important when dye molecules are in an adsorbed state on the catalyst surface [26].

$$CR + h\nu \rightarrow CR(h^+) + CR(e^-) \quad (6)$$

$$CR(e-)_{CB} + ZnFe_2O_4@MnO \rightarrow ZnFe_2O_4@MnO(e^-) + CR \quad (7)$$

$$ZnFe_2O_4@MnO(e^-) + O_2 \rightarrow ZnFe_2O_4@MnO + O_2\cdot^- \quad (8)$$

$$CR(h+)_{VB} + OH^- \rightarrow CR + OH^\cdot \quad (9)$$

$$O_2^{\cdot-} + 2H_2O + e^- \rightarrow 3OH^- + OH^\cdot \quad (10)$$

$$O_2^{\cdot-} + OH^\cdot + CR \rightarrow CO_2 + H_2O \quad (11)$$

CONCLUSION

In conclusion, magnetically separable $ZnFe_2O_4$@MnO and $MnFe_2O_4$@ZnO photocatalysts were successfully synthesized through a facile

Table 5. Rate constant of reaction kinetic for $ZnFe_2O_4$@MnO photocatalytic degradation by Congo red in different conditions.

pH	Initial CR solution concentration, mg/l	Photocatalyst loading, g	k , min^{-1}	R^2
13	50	0.05	0.0264	0.9879
13	50	0.10	0.0371	0.9877
13	50	0.15	0.0284	0.9919
13	50	0.20	0.0250	0.9833

Table 6. Rate constant of reaction kinetic for $MnFe_2O_4$@ZnO photocatalytic degradation by Congo red in different. conditions.

pH	Initial CR solution concentration, mg/l	Photocatalyst loading, g	k , min^{-1}	R^2
13	50	0.05	0.0243	0.9890
13	50	0.10	0.0324	0.9962
13	50	0.15	0.0251	0.9890
13	50	0.20	0.0218	0.9880

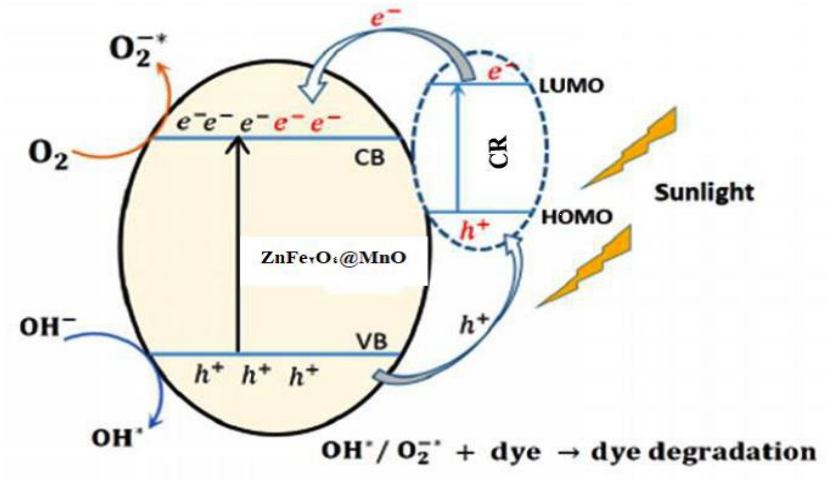

Fig. 20. Photocatalytic mechanism of $ZnFe_2O_4$@MnO photocatalyst.

hydrothermal method. The photocatalysts were investigated by FESEM, EDAX, XRD, UV-DRS and VSM. The effect of reaction time, pH, and and loading of $ZnFe_2O_4$@MnO and $MnFe_2O_4$@ZnO nanocomposites on degrading the CR were studied. Regarding the results of photocatalytic, the amount of the catalyst (0.1 g L^{-1}) and initial concentration of CR (50 mg L^{-1}) with pH=13-14 was considered as the best for Congo red degradation. The experimental data were adequated by calculating the pseudo-first-order kinetic. The prepared $ZnFe_2O_4$@MnO catalyst revealed significantly enhanced photocatalytic performance toward CR degradation in 35 min of under visible light irradiation compared to that of $MnFe_2O_4$@ZnO catalyst. The photocatalytic experimental results demonstrated that in the presence of 0.10g $ZnFe_2O_4$@MnO and $MnFe_2O_4$@ZnO degrade Congo red dye as a hazardous pollutant under visible light irradiation in the same reaction condition by 98.50 % and 90.32 % respectively. VSM measurements confirmed the superparamagnetic behavior of the synthesized samples at room temperature and the effect of crystallite size on the magnetic properties. The plot of the Kubelka-Munck function revealed the optical bandgap energy of $ZnFe_2O_4$@MnO is relatively less than that of $MnFe_2O_4$@ZnO nanoparticle. Thus the present work concludes that the magnetic and optical properties of synthesized $ZnFe_2O_4$@MnO nanoparticles and the photocatalytic property of $ZnFe_2O_4$@MnO nanoparticles makes the nanocomposites promising candidates for the solution of a variety of environmental problems.

ACKNOWLEDGEMENT

We thank science and research Branch, Islamic Azad University, Tehran, for supporting this study and Iran Nanotechnology Initiative.

DISCLOSURE STATEMENT

All authors declare that they have no conflict of interest in the publication of this manuscript.

REFERENCES

1. Houas A., Lachheb H., Ksibi M., Elaloui E, Guillard C., Herrmann J. M., (2001), Photocatalytic degradation pathway of methylene blue in water. *Appl. Catal. B: Environm*. 31: 145-157.
2. Konstantinou I. K., Albanis T. A., (2004), TiO_2-assisted photocatalytic degradation of azo dyes in aqueous solution: kinetic and mechanistic investigations: a review. *Appl. Catal. B: Environm*. 49: 1-14.
3. Zhu H., Jiang R., Xiao L., Chang Y., Guan Y., Li X., Zeng G., (2009), Photocatalytic decolorization and degradation of Congo Red on innovative crosslinked chitosan/nano-CdS composite catalyst under visible light irradiation. *J. Hazard. Mater.* 169: 933-940.
4. Feng Q., Li S., Ma W., Fan H. J., Wan X., Lei Y., Qin B., (2018), Synthesis and characterization of Fe_3O_4/ZnO-GO nanocomposites with improved photocatalytic degradation methyl orange under visible light irradiation. *J. Alloys and Comp.* 737: 197-206.
5. Özacar M., Şengil I. A., (2003), Adsorption of reactive dyes on calcined alunite from aqueous solutions. *J. Hazard. Mater.* 98: 211-224.
6. Lam S. M., Sin J. C., Abdullah A. Z., Mohamed A. R., (2012), Degradation of wastewaters containing organic dyes photocatalysed by zinc oxide: A review. *Desalinat. Water Treatment*. 41: 131-169.
7. Hisaindee S., Meetani M. A., Rauf M. A., (2013), Application of LC-MS to the analysis of advanced oxidation process (AOP) degradation of dye products and reaction mechanisms. *TrAC Trends in Anal. Chem.* 49: 31-44.

8. Gopalakrishnan A., Krishnan R., Thangavel S., Venugopal G., Kim S. J., (2015), Removal of heavy metal ions from pharma-effluents using graphene-oxide nanosorbents and study of their adsorption kinetics. *J. Indus. Eng. Chem.* 30: 14-19.
9. Balu A. M., Baruwati B., Serrano E., Cot J., Garcia-Martinez J., Varma R. S., Luque R., (2011), Magnetically separable nanocomposites with photocatalytic activity under visible light for the selective transformation of biomass-derived platform molecules. *Green Chem.* 13: 2750-2758.
10. Gupta V. K., Yola M. L., Eren T., Kartal F., Çağlayan M. O., Atar N., (2014), Catalytic activity of Fe@Ag nanoparticle involved calcium alginate beads for the reduction of nitrophenols. *J. Molecul. Liq.* 190: 133-138.
11. Gurumoorthy M., Parasuraman K., Anbarasu M., Balamurugan K., (2015), Synthesis and characterization of $MnFe_2O_4$ nanoparticles by hydrothermal method. *Nano Vision*. 5: 39-168.
12. Sinthiya M. M. A., Ramamurthi K., Mathuri S., Manimozhi T., Kumaresan N., Margoni M. M., Karthika, P. C., (2015), Synthesis of Zinc Ferrite ($ZnFe_2O_4$) nanoparticles with different capping agents. *Int. J. Chem. Tech. Res*. 7: 2144-2149.
13. Tran F., Blaha P.,. (2009), Accurate band gaps of semiconductors and insulators with a semilocal exchange-correlation potential. *Phys. Rev. Lett.* 102: 226401-226405.
14. Liu X., Chen C., Zhao Y., Jia B., (2013), A review on the synthesis of manganese oxide nanomaterials and their applications on lithium-ion batteries. *J. Nanomater.* 2013: Article ID 736375, 7pages.
15. Choi K., Kang T., Oh S. G., (2012), Preparation of disk shaped ZnO particles using surfactant and their PL properties. *Mater. Lett.* 75: 240-243.
16. Sinthiya M. M. A., Ramamurthi K., Mathuri S., Manimozhi T., Kumaresan N., Margoni M. M., Karthika P. C., (2015), Synthesis of Zinc Ferrite ($ZnFe_2O_4$) nanoparticles with different capping agents. *Int. J. Chem. Tech. Res*. 7: 2144-2149.
17. Aslibeiki B., Kameli P., Salamati H., (2013), The role of Ag on dynamics of superspins in $MnFe_{2-x}$ Ag x O_4 nanoparticles. *J. Nanopart. Res.* 15: 1430-1436.
18. Suwanchawalit C., Somjit V., (2015), Hydrothermal synthesis of magnetic $CoFe_2O_4$-Graphene nanocomposite with enhanced photocatalytic performance. *Digest. J. Nanomater. Biostruc.* 10: 769-777.
19. Vlazan P., Stefanescu M., Barvinschi P., Stoia M., (2012), Study on the formation of $CoxFe_{3-x}O_4$ system using two low temperature synthesis methods. *Mater. Res. Bullet.* 47: 4119-4125.
20. Li N., Zheng M., Chang X., Ji G., Lu H., Xue L., Cao J., (2011), Preparation of magnetic $CoFe_2O_4$-functionalized graphene sheets via a facile hydrothermal method and their adsorption properties. *J. Solid State Chem.* 184: 953-958.
21. Naseri M. G., Saion E. B., (2012), Crystalization in spinel ferrite nanoparticles. *In Advances in Crystallization Processes.* 349-380.
22. Sathishkumar P., Mangalaraja R. V., Anandan S., Ashokkumar M., (2013), $CoFe_2O_4/TiO_2$ nanocatalysts for the photocatalytic degradation of reactive red 120 in aqueous solutions in the presence and absence of electron acceptors. *Chem. Eng. J.* 220: 302-310.
23. Guo H., Chen J., Weng W., Wang Q., Li S., (2014), Facile template-free one-pot fabrication of $ZnCo_2O_4$ microspheres with enhanced photocatalytic activities under visible-light illumination. *Chem. Eng. J.* 239: 192-199.
24. Arunadevi R., Kavitha B., Rajarajan M., Suganthi A., Jeyamurugan A., (2018), Investigation of the drastic improvement of photocatalytic degradation of Congo red by monoclinic Cd, Ba-CuO nanoparticles and its antimicrobial activities. *Surf. Interf.* 10: 32-44.
25. Chin Boon O., Mohammad A. W., Rohani R., Ba-Abbad M. M., Hairom N. H. H., (2016), Photocatalytic degration of hazardous congo red using low- temperature synthesise of zinc oxide nanoparticles. *Proc. Safety Environmen. Protec.* 104: 549-557.
26. Shinde D. R., Tambade P. S., Chaskar M. G., Gadave K. M., (2017), Photocatalytic degradation of dyes in water by analytical reagent grades ZnO, TiO_2 and SnO_2: A comparative study. *Drink. Water Eng. Sci.* 10: 109-117.